ORIGINAL RESEARCH PAPER

Evaluation and synthesis of Nano-pore Hydroxysodalite (HS) zeolite membranes: Application to pervaporation of Ethanol/water mixture

Mansoor Kazemimoghadam[1,]*, Zahra Amiri Rigi[2]

[1]Department of Chemical Engineering, Malek-Ashtar University of Technology, Tehran, Iran
[2]Department of Chemical Engineering, South Tehran Branch, Islamic Azad University, Tehran, Iran

ABSTRACT

Effect of crystallization time and temperature on the membrane structure and performance has been investigated for Nano-pore Hydroxysodalite (HS) zeolite membranes. Molar composition of the starting gel of the HS zeolite membranes were: SiO_2/Al_2O_3=1.0-5.0, Na_2O/Al_2O_3=15-65, and H_2O/Al_2O_3=500-1500. X-ray diffraction (XRD) patterns of the membranes exhibited peaks corresponding to the support and the zeolite. The crystal species was characterized by XRD and the morphology of the supports subjected to crystallization was characterized by Scanning Electron Microscopy (SEM). Separation performance of HS zeolite membranes was studied for water-Ethanol mixtures using pervaporation (PV). The membranes showed good selectivity towards water in the water-Ethanol mixtures. Water permeates faster because of its preferential adsorption into the Nano-pores of the hydrophilic zeolite membrane. In PV of water-Ethanol mixtures, the membrane exhibits a hydrophilic behavior, with a high selectivity towards water and a good flux. The best flux and separation factor of the membranes were 2.05 kg/m².h and 10000, respectively. Effect of operating condition (temperature, flow rate and pressure) on the membrane performance was investigated for HS zeolite membranes grown onto seeded mullite supports. Finally, a comprehensive 2D model was developed for the PV of water-Ethanol mixture through HS zeolite membrane using Finite Element Method (FEM). Effect of varying dimensional factors, temperature and feed flow rate on the PV performance was studied. The proposed model was masterfully capable of predicting concentration distribution within two sub-domains of feed and membrane.

Keywords: *Ethanol; FEM; Hydroxysodalite; Pervaporation; Zeolite Membrane*

INTRODUCTION

Ethanol is a very important and commonly used solvent in biopharmaceutical and chemical industries. It is widely applied as a disinfectant in medical products, as fuel in rockets and engines and as a feedstock for synthesis of other organic chemicals such as acetic acid, Butanol and ethyl ester [1-3]. Thus, it is very important to treat ethanol waste to separate this valuable material and prevent its wasting.

Separation of Ethanol from its aqueous mixture can be performed through conventional distillation. However, this process is very difficult mainly because Ethanol forms an azeotrope with water once it reaches 89.4 mole % at 78°C and atmospheric pressure. Thus, azeotropic distillation must be applied for this purpose. Nonetheless, azeotropic distillation is more energy demanding than traditional distillation. Besides, benzene, a highly carcinogenic and toxic substance will be produced in this process, which has been considered a major health concern [4, 5].

* Corresponding Author Email: *mzkazemi@gmail.com*

Instead, pervaporation is an economical filtration technique compared to conventional distillation, especially in processes involving azeotropes, isomers and removal or recovery of trace substances. This is mainly because that only a fraction of the solution that needs to be separated is vaporized in pervaporation. Additionally, high flux rate of PV makes this method an efficient purification technique, resulting in energy cost saving. Table 1 shows the amount of energy demanded by different separation techniques in ethanol dehydration. In terms of energy requirement, pervaporation is an obvious choice in Ethanol–water filtration [6-10]. Aside from consuming lower energy, capital cost of PV operation is considerably lower which makes it more effective compared to distillation.

PV has attracted great attention not only for its cost-effective features, but also for its simplicity and safe operation. In fact, the main tools needed for PV are a vacuum pump creating the required driving force and a membrane separating the solution. Furthermore, pervaporation eliminates the use of toxic materials such as benzene and thus is a promising alternative for energy consuming distillation systems in filtering azeotropic mixtures. Hence, relatively mild operating conditions and high effectiveness make PV an appropriate technique for such separations [11-14].

In general, polymeric membranes can be applied for PV dehydration of organic solutions such as Ethanol-water mixture. However, these membranes are not suitable for applications involving harsh chemicals, due to the membrane chemical instability. In this regard, recent chemical-and-temperature resistant hydrophilic ceramic membranes have been developed, making it possible to overcome the limitations of polymeric membranes [15-17]. Since zeolites are most hydrophilic and have well-defined open crystal structures with a pore size of several angstroms, they are another candidate for the pervaporation dehydration of highly concentrated ethanol aqueous solution. These unique structural characteristics and hydrophilic nature have rendered zeolite materials possessing pronounced molecular sieving effect and selective adsorption capability (i.e., appreciated separation performance). Therefore, zeolites can be extensively used in removal of volatile organic chemicals from air streams, separation of isomers and mixtures of gases, shape-selective catalysis and ion exchange. Zeolitic membranes offer several advantages over polymeric ones. Firstly, they do not swell significantly compared to the polymeric membranes. Secondly, they have uniform molecular-sized pores that provide differential transport rates and molecular sieve effects. Thirdly, the zeolitic structures are more chemically stable and tolerant to severe separation conditions such as strong solvents or low pH solutions. Last but not least, zeolites are thermally stable up to high temperatures of 1000°C [18, 19].

In pervaporation the feed mixture is contacted with a perm-selective nonporous membrane. Separation is generally explained by the steps of sorption into, diffusion through and desorption from the membrane. The latter is usually considered fast and taking place at equilibrium while diffusion is kinetically controlled and the slowest step of the process. Permeation is dependent on the sorption and diffusion steps. The driving force for the separation is created by maintaining a pressure lower than the saturation pressure on the permeate side of the membrane. The mechanism of filtration is usually described in terms of sorption-diffusion processes [20-23].

Extensive studies have been conducted for mass transfer modeling of PV systems [24-31]. Recently Rezakazemi et al. (2011) proposed a model for PV separation of water/ethylene glycol solution based on solving equations of mass and momentum conservation (Navier-Stokes equations) with Finite Element Method (FEM) [26]. Effect of temperature and velocity was investigated in their research and their results were in good agreement with experimental data. After Rezakazemi et al., Moulik et al. (2015) used the same approach and developed a steady state model to predict mass transfer of MMH and UDMH solutions by pervaporation [24]. Their results were also in reasonable accordance with empirical data. Nonetheless, their model was

Table 1: Energy requirements for ethanol dehydration [10]

Purification (Wt. %)	Energy required (kJ/kg EtOH)	Process
8.0–99.5	10376	Distillation
95.0–99.5	3305	Azeotropic distillation
95.0–99.5	423	Pervaporation

174

J. Water Environ. Nanotechnol., 3(2): 173-190 Spring 2018

not comprehensive, since they only modeled the membrane section of the module. The effect of dimensional factors relating to the geometry of the system is also neglected in their study.

So far, few attempts have been done to simulate highly concentrated Ethanol/water pervaporation using FEM technique, lacking prediction of water concentration distribution within the membrane section [32, 33]. The effect of various dimensional factors relating to the geometry of the membrane system and feed flow rates on water concentration distribution was also neglected. The objective of this study was to develop robust membranes as well as effective models for providing a deep insight into the dehydration of Ethanol/water mixtures with PV technology. In this regard, Nano-pore HS zeolite membranes were fabricated and then used to concentrate water/Ethanol mixtures. The membranes were basically made of an active HS layer deposited over a ceramic porous mullite support. Zeolite HS layers were coated on the external surface of the porous tubular mullite supports using hydrothermal method. These membranes were successfully utilized for the dehydration of the water/Ethanol mixtures. The achieved flux rates were remarkably high due to the hydrophilic nature of the membrane. The active HS layer is also responsible for high separation factors achieved in PV of Ethanol mixtures. A mathematical model based on CFD technique was finally proposed and the effect of different membrane's dimensions, temperatures and feed flow rates on water concentration was investigated, which can be hardly seen in the literature. Proposed model was distinctively capable of predicting concentration distribution in both membrane and feed sub-domains and provided a perfect understanding of the effect of various operating conditions on the membrane performance.

EXPERIMENTAL
Zeolite membrane synthesis
Coating of the support with seeds

Conventional zeolite synthesis includes pre coating of seeds and then crystallization. Detailed information about support preparation can be found elsewhere [34-36]. Adding seed crystals to this crystallization system resulted in increased crystallization rate. Enhanced rate might be due to simply increasing the rate at which solute is integrated into the solid phase from solution due to the increased available surface area, but also might

be the result of enhanced nucleation of new crystals. The secondary nucleation mechanism referred to as initial breeding results from microcrystalline dust being washed off seed crystal surfaces in a new synthesis batch. These microcrystalline fragments grew to observable sizes, and resulted in greatly enhanced crystallization rates due to remarkably increased crystal surface area compared to the unseeded system. Consequently, it is expected that addition of seed crystals to a synthesis system will introduce sub-micron sized crystallites into the system that will serve as nuclei.

As described above, porous mullite tubes (homemade) were used as the support. The external surface of the supports was polished with 600-grit sandpapers, and then the support was washed and cleaned with distilled water in a microwave heater for 5 min to remove loose particles created during polishing. Then, supports were dried at 100°C for 3h.

In order to form a thin and uniform zeolite membrane on the mullite support, the nucleation seeds should be small and uniform in size. In order to inhibit the formation of the zeolites into the support pores, the seeds should not penetrate into the pores. High purity nucleation seeds were synthesized by hydrothermal method. Size of the seeds was about 2 μm. The seeds must be dispersed homogeneously on the support surface and the amount of seeds on the support surface must not be too much. Otherwise, the synthesized zeolite membrane is heterogeneous or too thick.

The seeded supports were prepared by dipping the mullite supports in an 8% NaA zeolite suspension in a single step. 8% NaA zeolite suspension was prepared by mixing 8 g NaA zeolite in 92 ml distilled water. After dipping procedure, the supports were dried at 100°C for 3 h.

HS zeolite synthesis

Thin zeolite HS membrane layers were grown hydrothermally over the external surface of the mullite supports. HS zeolite membranes were fabricated by in situ crystallization on the outer surface of the porous mullite tubes. Si source was sodium silicate and Al source was sodium aluminates. Synthesis solution was made by mixing aluminates and silicate solutions. NaOH was dissolved in distilled water. The solution was divided into two equal volumes and kept in polypropylene bottles. Aluminates solution was prepared by adding sodium aluminates to one part of the

NaOH solution. It was mixed until cleared. Silicate solution was prepared by adding sodium silicate to another part of the NaOH solution. Silicate solution was then poured into aluminates solution and well mixed until a thick homogenized gel was formed. Molar composition of the starting gel of the HS zeolite membranes was SiO_2/Al_2O_3=1.0-5.0, Na_2O/Al_2O_3=15-65, H_2O/Al_2O_3=500-1500 [37-40].

Crystallization was carried out in an oven at temperatures of 70, 100 and 130 °C for 6, 12 and 24 h. Then, the samples were taken and the synthesized membranes were washed several times with distilled water. The samples were then dried at room temperature for 12 h in air. The zeolite membranes were used for dehydration of Ethanol aqueous mixture. Ethanol mixtures (90 wt%) were applied and experiments were carried out at room temperature (25°C) within a period of 30-60 min. Permeate concentrations were measured using GC (TCD detector, Varian 3400, carrier gas: hydrogen, column is polyethylene glycol, sample size: 5 micron, column and detector temperatures: 120°C-150°C, detector flow rate: 15 ml/min, carrier flow: 5 ml/min, column pressure: 1.6 kPa, GC input pressure: 20 kPa). Performance of PV was evaluated using values of total flux (kg/m².h) and separation factor (dimensionless).

The phases Mullite, Cristobalite and SiO_2 identification was performed by X-ray diffraction (Philips PW1710, Philips Co., Netherlands) with CuKα radiation. Morphology of the support and the membrane was examined by Scanning Electron Microscopy (JEM-1200 or JEM-5600LV equipped with an Oxford ISIS-300 X-ray disperse spectroscopy (EDS)).

Zeolite structure and transport mechanisms

The structure of the zeolite HS is shown in Fig. 1 [41]. As can be seen from the figure, the aluminosilicate framework of the zeolite HS is generated by placing truncated octahedrons (b-cage) at eight corners of a cube and each edge of the cube is formed by joining two b-cages. Each b-cage encloses a cavity with a free diameter of 0.66 nm and each unit cell encloses a larger cavity (a-cage). There are two interconnecting, three-dimensional channels in the zeolite HS. Firstly, there are connected a-cages, separated by 0.3 nm apertures. Secondly, b-cages are present alternating with a-cages separated by 0.22 nm apertures. Thus, molecules smaller than 0.3 nm in diameter can diffuse easily through the Nano-pores of the zeolite. In addition, position of the sodium ions in unit cells is important since these ions act as the sites for water sorption and transport through the membrane. For a typical zeolite, a unit cell having the composition of Na_6 $[Al_6Si_6O_{24}]$ $(OH)_2$ (1.5 H_2O), eight (out of 12) sodium ions are located inside an a-cage and four ions are located in b-cages [41]. Transport of solvent species (mainly water) through zeolite matrix comprises of three steps: (i) strong adsorption of the species into a cage from the feed side, (ii) surface diffusion of the species from cage to cage and (iii) vaporization of the species to permeate side. Normally, any physical adsorption process includes both Vander Waals dispersion-repulsion forces and electrostatic forces comprising of polarization, dipole and quadrupole interactions. However, since the zeolites have an ionic structure, the electrostatic forces become very large in adsorption of polar molecules like H_2O.
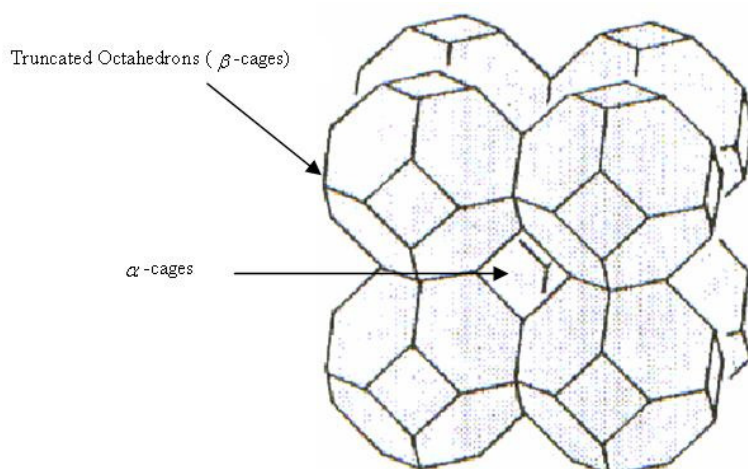

Fig. 1: Repeating unit of zeolite HS [41]

176

J. Water Environ. Nanotechnol., 3(2): 173-190 Spring 2018

This effect is manifested in the fact that the heat of the adsorption of the water into zeolitic adsorbents is unusually high (25–30 kcal/mole).
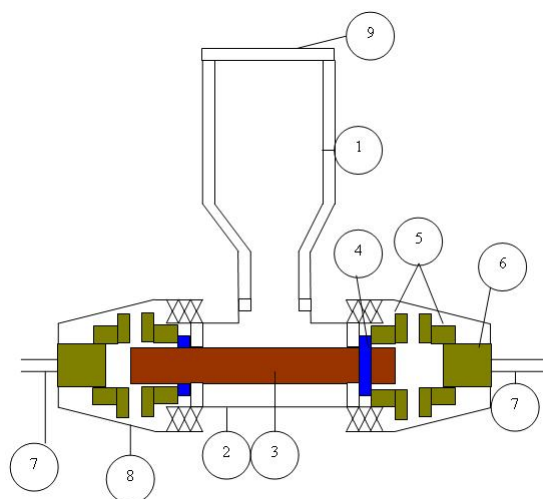
Pervaporation tests

The zeolite membranes were used for long-term dehydration of Ethanol. Experiments were conducted at a temperature of 30°C and a pressure of 1.5 mbar at the permeate side within a period of 30-60 min. Inner radius and length of the membrane module was 5 and 110 mm, respectively. Membrane effective surface area was 44 cm².

Pervaporation setup is presented in Fig. 2(a) and (b) [34, 42]. Any change of feed concentration due to the permeation is negligible because the amount of pe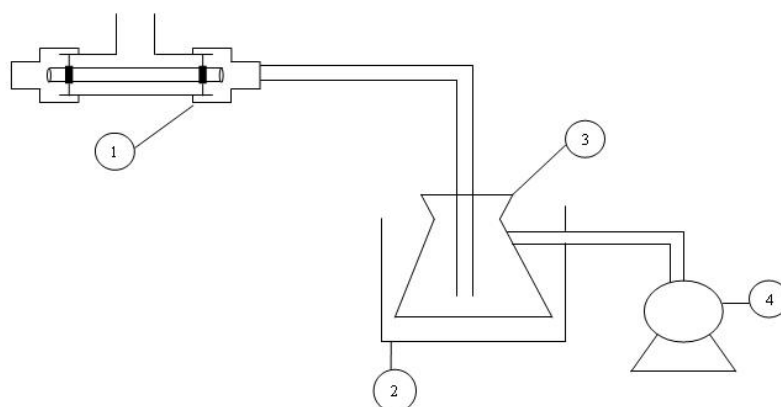rmeate is small (max 2 ml) compared to the total feed volume in the system (0.5 lit). A three stage diaphragm vacuum pump (vacuubrand, GMBH, Germany) was employed to evacuated the permeate side of the membrane to a pressure of approximately 1.5 mbar while the feed side was kept at room pressure. The permeate side was connected to a liquid nitrogen trap via a hose to condense the permeate (vapor). Permeate concentrations were measured by a GC (TCD detector, Varian 3400).

Theory

Fig. 3 represents the schematic diagram of the model domain used in the simulation. Feed solution containing a mixture of 90 wt. % Ethanol and 10 wt. % water flows tangentially through the upper side of the membrane system (z=0). The feed

(a) Pervaporation cell; 1- feed tank, 2-membrane module, 3- membrane, 4- O-ring, 5- Teflon fitting, 6- stainless steel vacuum fitting, 7- vacuum hose, 8- cap, 9- feed tank cap

(b) Pervaporation setup; 1- PV cell, 2- liquid nitrogen trap, 3- permeate container, 4- three stage vacuum pump

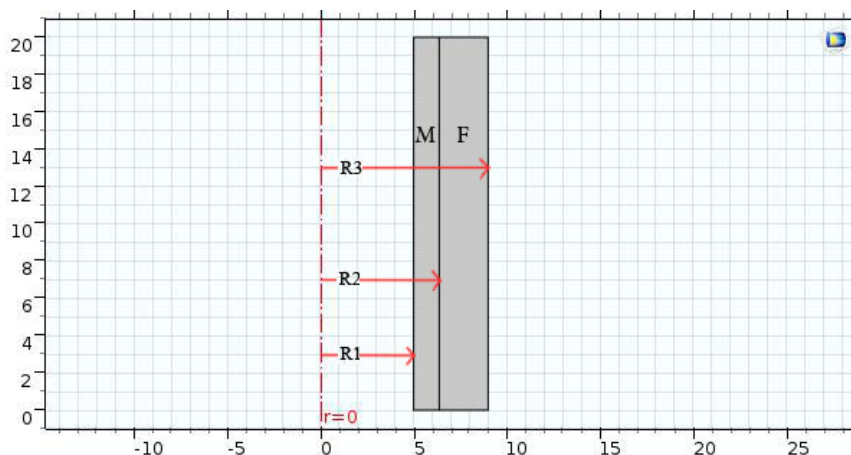Fig. 2: Filtration system; (a) Pervaporation cell [34] and (b) Pervaporation setup [42]

J. Water Environ. Nanotechnol., 3(2): 173-190 Spring 2018

177

Fig. 3: Geometry of the PV system used in the simulation

exits at z=L (membrane length) and recirculates inside the system.

The main assumptions to develop the numerical simulation are as follows:

❖ Steady state and isothermal conditions.
❖ No chemical reaction occurs in feed stream.
❖ Feed solution flows only in the z direction.
❖ Laminar feed flow in the membrane system.
❖ Thermodynamic equilibrium considered at the interface of feed and membrane.
❖ Small amount of Ethanol permeates through the membrane.
❖ Mass transfer resistance of the support layer was assumed to be negligible.
❖ Fouling and concentration polarization effects on the PV of Ethanol/water solution are negligible.
❖ The fluid is incompressible.
❖ Feed viscosity is constant.

Although the diffusive mass transfer in the direction of flow (z direction) is small due to the convective flux in this direction, it is not neglected compared to diffusive mass transfer in the r direction. Therefore, axial and radial diffusions inside the membrane and feed phase are considered in the continuity equations. Moreover, the small permeation of Ethanol through the membrane is considered in the simulation by applying selectivity equation (Eq. (1)). The penetration of Ethanol through the selective membrane is described by the following equation:

$$S = \frac{x_{Ethanol}}{x_{water}} \times \frac{y_{water}}{y_{Ethanol}} \qquad (1)$$

The concentration of Ethanol in the permeate side ($y_{Ethanol}$) must be determined by trial and error method. In this method, an initial value for $y_{Ethanol}$ is guessed. Then the water concentration in the permeate side will be calculated using model equations. This calculated value then must be compared with the guessed value. If the difference between the old and new values is less than a determined error, the guessed Ethanol concentration is considered as the correct concentration. Otherwise, another guess must be made for $y_{Ethanol}$.

Mass transport in the membrane system is described using continuity equation. The following equation presents the differential form of this equation [43]:

$$\frac{\partial C_w}{\partial t} + \nabla \cdot (-D_w \nabla C_w + U \cdot C_w) = R \qquad (2)$$

Where C_w denotes water concentration (mol/m³), D_w denotes water diffusion coefficient (m²/s), U denotes the velocity vector (m/s) and R denotes the reaction term (mol/m³.s). Since no chemical reaction takes place in the Ethanol/water PV, the reaction term is zero. Continuity equation was defined and solved in COMSOL Multiphysics 5.2 by adding a "transport of diluted species" physic to the model domain. Velocity distribution was obtained by solving Navier-Stokes equations for momentum balance simultaneously with continuity equation in the feed side. This was done by adding a "laminar flow" physic to the whole model in COMSOL Multiphysics 5.2. The following equation describes the momentum conservation equation [43]:

$$\rho \frac{\partial u}{\partial t} + \rho (u \cdot \nabla) u = \nabla \cdot [-P + \mu (\nabla u + (\nabla u)^T)] + F_b \qquad (3)$$

$$\nabla \cdot (u) = 0 \tag{4}$$

Where u denotes z-component of the velocity vector (m/s), ρ denotes feed density (kg/m^3), P denotes pressure (Pa), μ denotes feed viscosity (Pa.s) and F_b denotes a body force (N).

Feed phase simulation

By applying mentioned assumptions to the Eq. (2), steady state form of the continuity equation for water mass transport in the feed side is obtained:

$$-\frac{1}{r}\frac{\partial}{\partial r}\left(D_w r \frac{\partial C_{w-f}}{\partial r}\right) - \frac{\partial}{\partial z}\left(D_w \frac{\partial C_{w-f}}{\partial z}\right) + u \frac{\partial C_{w-f}}{\partial z} = 0 \tag{5}$$

The simplified form of the momentum transport equations considering above assumptions will be as follows:

$$\rho\left(u\frac{\partial u}{\partial z}\right) - \frac{1}{r}\frac{\partial}{\partial r}\left(r\mu\frac{\partial u}{\partial r}\right) - \frac{\partial}{\partial z}\left(\mu\frac{\partial u}{\partial z}\right) = -\frac{\partial P}{\partial z} \tag{6}$$

$$\frac{\partial u}{\partial z} = 0 \tag{7}$$

r and z denote radial and axial coordinates, respectively.

The initial conditions for mass and momentum conservation equations are as below:

at t=0, $C_{w-f}=C_{0,w}$ and $u=u_0$ $\tag{8}$

Where C_{w-f} is water concentration in feed phase, $C_{0,w}$ is its initial value and u_0 is the initial velocity of the feed flow.

The boundary conditions for mass conservation equations in the feed phase are as follows:

at z=L, Outflow condition $\tag{9}$

at z=0, $C_{w-f} = C_{0,w}$ (Inlet boundary) $\tag{10}$

at r=R$_3$, $\frac{\partial C_{w-f}}{\partial z} = 0$ (No flux condition) $\tag{11}$

At the interface of the membrane-feed, the equilibrium condition is assumed:

at r= R$_2$, $C_{w-f} = \frac{C_{w-m}}{n}$ $\tag{12}$

In which C_{w-m} is water concentration in membrane section and n is partition coefficient obtained from selectivity equation as follows:

$$n = \frac{y_{Ethanol}}{x_{Ethanol}} \times S = \frac{C_{w-m}}{C_{w-f}} \tag{13}$$

As mentioned earlier, permeate concentration of Ethanol must be obtained using trial and error method and then will be placed in the above equation.

The boundary conditions for momentum transfer equations are as follows:

at z=0, u=u$_0$, (Inlet boundary) $\tag{14}$

At the outlet, the pressure is atmospheric pressure:

at z=L, P=P$_{atm}$, (Atmospheric pressure) $\tag{15}$

At r=R$_2$ and R$_3$, u=0 (No slip condition) $\tag{16}$

Membrane phase simulation

Mass transport of water in membrane is controlled only by diffusion mechanism. Therefore, the steady state continuity equation for water can be written as:

$$-\frac{1}{r}\frac{\partial}{\partial r}\left(D_m r \frac{\partial C_{w-m}}{\partial r}\right) - \frac{\partial}{\partial z}\left(D_m \frac{\partial C_{w-m}}{\partial z}\right) = 0 \tag{17}$$

where D_m is water diffusion coefficient in membrane (m^2/s).

Membrane phase boundary conditions are given as:

at r=R$_2$, $C_{w-m} = n \times C_{w-f}$ (Equilibrium condition) $\tag{18}$

at r= R$_1$, $C_{w-m} = 0$ (Dry membrane condition) $\tag{19}$

at z=0 and z=L, $\frac{\partial C_{w-m}}{\partial z} = 0$ (No flux condition) $\tag{20}$

At the permeate-membrane interface, water concentration assumed to be zero due to the vacuum applied on this boundary.

Numerical solution of the conservation equations

Set of model equations, including mass and momentum transfer equations in the membrane module along with suitable boundary conditions was solved using COMSOL Multiphysics software version 5.2. Finite element method (FEM) is applied by this software to solve conservation equations numerically. Previous simulations of

J. Water Environ. Nanotechnol., 3(2): 173-190 Spring 2018

179

membrane separation processes using FEM showed that this method is an accurate, valid and powerful technique for solving mass and momentum equations [24, 26, 30]. The computational time for solving the equations was about 400 s. "Extremely fine" mesh was used in the simulation which consisted of 106198 domain elements and 1879 boundary elements. Fig. 4 represents the meshes created by COMSOL Multiphysics 5.2 software. Due to the considerable difference between z and r dimensions, a scaling factor equal to 5.5 was used in the z direction. Therefore, the results were reported in dimensionless height.

RESULTS AND DISCUSSION
Gel Composition

As mentioned earlier, zeolites could be synthesized by the hydrothermal method. The versatility of the hydrothermal chemistry owes much to the mineralizing role of the water. The factors that promote reactivity in aqueous magmas include:
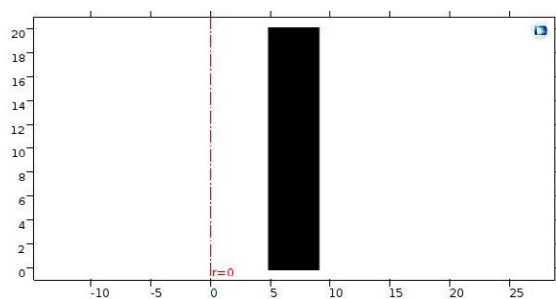
1. Stabilization of porous lattices as zeolites by acting as space fillers, referred to above.

2. Through its presence, especially at high pressures, water may be incorporated into hydrous glasses, melts, and solids. Through chemisorptions into siliceous materials, Si-O-Si, and Al-O-Si bonds hydrolyze and re-form. Chemical reactivity is enhanced and magma viscosity is lowered.

3. High pressures of water can modify phase equilibrium temperatures.

4. Water is a good solvent, a property that assists disintegration of solid components of a mixture and facilitates their transport and mixing.

Water is important as a guest molecule in zeolite structures with relatively high Al contents and consequently, aqueous media favor their formation w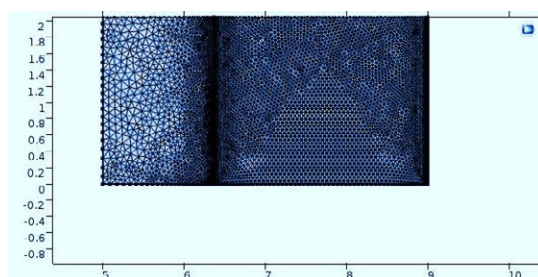hile salts have a parallel role in the stabilization of zeolite structure. In general, the zeolitic water can be removed leaving the unchanged hydrous zeolite. In hydrothermal systems, the good solvent powers of water promote mixing, transport of materials, and facilitate nucleation and crystal growth. Water stabilizes zeolite structures by filling the cavities and forming a type of solid solution. The stabilizing effect is such that the porous aluminosilicates will not form in the absence of a guest molecule, which may be a salt molecule as well as water. However, the water concentration or the degree of dilution is important for the synthesis of HS which can crystallize out of gels with an extremely wide range of H_2O/Al_2O_3 ratios (from 500 to 1500).

Overall, the Na_2O or alkalinity of the media plays a vital role in crystal growth, materials synthesis, preparation and processing. It influences the super saturation, kinetics, morphology, shape, size, and crystallinity of the particles or materials as the OH anions fulfill the crucial role of mineralizing agent. The Na_2O is influenced by the reactants and their concentrations or ratios followed by temperature and time. Further, with the introduction of organics, the alkalinity changes rapidly in the system. Hence, alkalinity is the key parameter in determining the crystallization rate. An increase in OH concentration will generally bring about an accelerated crystal growth and a shortened induction period before viable nuclei are formed. In zeolite synthesis, pH of the alkaline solution is usually between 8 and 12. The major role of pH is to bring the Si and Al oxides or hydroxides into solution at an adequate rate.

To study the effects of gel composition on HS zeolite membrane performance, the membranes were synthesized at different compositions (SiO_2/Al_2O_3=1.0-5.0, Na_2O/Al_2O_3=15-65, H_2O/Al_2O_3=500-1500) for duration of 12 h and at temperature of 100°C. It must be also mentioned

(a) Complete mesh

(b) Magnification of a segment of the complete mesh

Fig. 4: Mesh used in the simulation; (a) Complete mesh and (b) Magnification of a segment of the complete mesh

180

J. Water Environ. Nanotechnol., 3(2): 173-190 Spring 2018

that three samples were prepared for each condition. The results were presented on average and the maximum deviation was less than 3%.

As seen in Table 2, HS zeolite membranes were successfully synthesized in ranges of $SiO_2/Al_2O_3=1.0$ to $SiO_2/Al_2O_3<2.5$, $Na_2O/Al_2O_3=15$-65, $H_2O/Al_2O_3>500$ to $H_2O/Al_2O_3=1500$.

In $H_2O/Al_2O_3<500$ ratio, HS zeolite membranes were not successfully synthesized because gel composition had not enough water for synthesis a homogenous gel. Moreover, $SiO_2/Al_2O_3>2.5$ ratio caused HS zeolite to transform to other zealots. It should be pointed out that 10000 is the highest measurable value using the GC at 90 wt.% Ethanol concentration as shown in Table 2.

Effect of temperature and time on the zeolite formation process

Temperature and time have a positive influence on the zeolite formation process which occurs over a considerable range of temperatures. A rise in temperature will increase both the nucleation rate and the linear growth rate. Therefore, the crystallinity of the samples normally increases in time. Concerning time, zeolite synthesis is governed by the occurrence of successive phase transformations. The thermodynamically least favorable phase will crystallize first and will be successively replaced in time by more stable phases. The best example is the crystallization sequence of amorphous → NaA → HS.

The temperature, however, can also influence the type of product that has to be crystallized. A rise in temperature leads to the crystallization of more dense products as the fraction of the water in the liquid phase, which has to stabilize the porous products by filling the pores' drops. Therefore, the existence of an upper limit for the formation of zeolites is to be expected. Use of nonvolatile pore space occupying (filling) species would, in principle, allow a high-temperature synthesis of open, porous structures. Temperature can obviously affect the rate of nucleation and crystal growth.

The linear rates of crystal growth and rates of nucleation both grow with rising temperatures.

To study the effect of crystallization time and temperature on the membrane performance, the membranes were synthesized at different temperatures (70, 100 and 130 °C) and different times (6, 12 and 24 h). As seen in Table 2, increasing crystallization time decreases water flux. However, there is no change in separation factor. This may be due to the fact that at a longer crystallization time a thicker membrane layer is formed. This causes water flux to decrease. This shows that the membranes behave very high selective. The results show that short crystallization time (6 h) is not enough to make an effective HS zeolite layer on the support (sample 13). This sample shows poor selectivity. The crystallization time in a range of 12-24 h was found to be very effective for making HS zeolite layer.

As observed in Table 2, increasing crystallization temperature increases water flux (samples 10, 11 and 12). In addition, it can be seen that there is no change in separation factor. This may be due to the fact that at higher crystallization temperature, a thinner layer is formed. It is because that at

Table 2: Flux and separation factor of HS zeolite membranes

Sample	Number of coating	SiO_2/Al_2O_3	Na_2O/Al_2O_3	H_2O/Al_2O_3	t (h)	T (°C)	Ethanol (%)	Flux $kg/m^2.h$	Separation factor	Flux*S.F
1	1	1.0	65	1000	12	100	90	0.750	>10000	7500
2	1	2.5	65	1000	12	100	90	1.140	176	200.64
3	1	5.0	65	1000	12	100	90	6.290	31	194.99
4	1	1.0	15	1000	12	100	90	0.227	>10000	2270
5	1	1.0	40	1000	12	100	90	0.624	>10000	6240
6	1	1.0	65	1000	12	100	90	0.750	>10000	7500
7	1	1.0	65	500	12	100	90	3.145	88	276.76
8	1	1.0	65	1000	12	100	90	0.750	>10000	7500
9	1	1.0	65	1500	12	100	90	1.224	>10000	12240
10	1	1.0	65	1000	12	70	90	0.681	>10000	6810
11	1	1.0	65	1000	12	100	90	0.750	>10000	7500
12	1	1.0	65	1000	12	130	90	2.05	>10000	20500
13	1	1.0	65	1000	6	100	90	1.0	26	26
14	1	1.0	65	1000	12	100	90	0.75	>10000	7500
15	1	1.0	65	1000	24	100	90	0.621	>10000	6210

J. Water Environ. Nanotechnol., 3(2): 173-190 Spring 2018

181

higher temperatures, the synthesis solution becomes heterogeneous and as a result, the HS zeolite layer becomes thinner. This also shows that the membranes behave very high selective. The crystallization temperature in a range of 70-130°C was found to be very effective for making the HS zeolite layer.
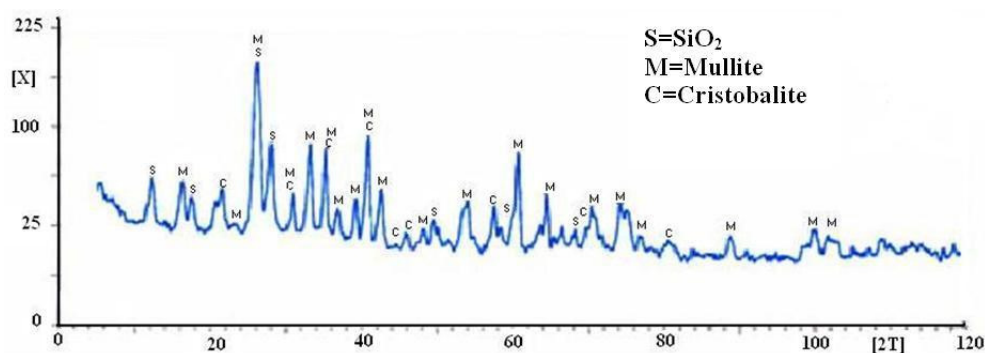
The results confirm that zeolite membranes synthesized at 130 °C for 12 h via a single stage process can be recommended for dehydration of dilute water/ Ethanol mixtures. The membranes are uniform and defect free and as a result, their separation factors are very high. Minimum synthesis time for the HS zeolite layer was found to be 12 h for making a uniform membrane.

Fig. 5(a) and (b) show XRD patterns of the mullite support and the HS zeolite membrane, respectively [42, 44]. The XRD pattern of HS zeolite membrane revealed that zeolite HS crystals w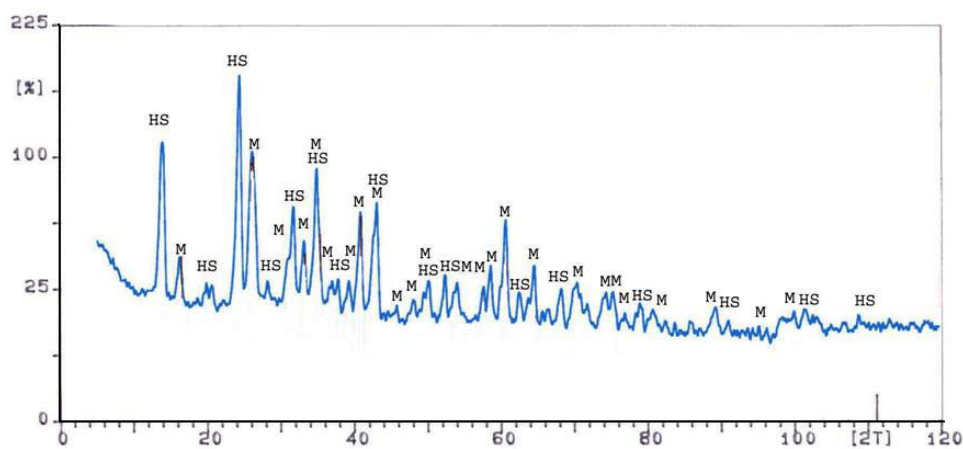ere formed. Fig. 6 shows SEM photographs of the mullite support (Fig. 6(a)) and the HS zeolite membrane (Fig. 6(b) and (c)). Porous structure of the support and thin layer of the membrane can be easily observed.

PV operating conditions

Effect of operating conditions on PV process was evaluated by cross flow PV pilot. The trans-membrane pressure was adjusted between 1 and 3 bar. The feed temperature was varied between 20 and 60 °C by means of a small heat exchanger employed into the feed tank. Feed rate was varied between 0.5 and 3 lit/min by means of centrifuge pumps and recycle lines. Permeate collected in a sample bottle was measured. The outlet flow of the cell could be led out of the system or returned to the tank. As shown in Table 3, effect of the feed flow rate on the permeate flux was measured at constant temperature (20°C) and constant pressure (1 bar). Increasing feed rate escalates the permeate

(a) XRD of the support

(b) XRD of the HS zeolite membrane

Fig. 5: XRD of the (a) Support [42] and (b) HS zeolite membrane [44]

182

J. Water Environ. Nanotechnol., 3(2): 173-190 Spring 2018

flux. As shown in Table 3, by increasing pressure the permeate flux grows. Increasing rate expands turbulence and hydrodynamic effects will result in growing permeate fluxes. Temperature is known as a main parameter. Increasing temperature reduces the dynamic viscosity. Table 3 shows the experimental data for the flux as a function of temperature. As seen, the flux increases with temperature. According to the results, it can be said the optimum operating conditions were 60°C, 3 bar and 3 lit/min.

Simulation results
Water concentration distribution

Fig. 7 (a) and (b) illustrates the surface water concentration distribution within two sub-domains of the membrane and feed, respectively. The Ethanol/water solution containing 10 wt. % water flows over the outer surface of the membrane module (z=0). Concentration profile within the feed side was measured by simultaneous solution of the continuity equations of mass and momentum using

(a) Support

(b) Membrane

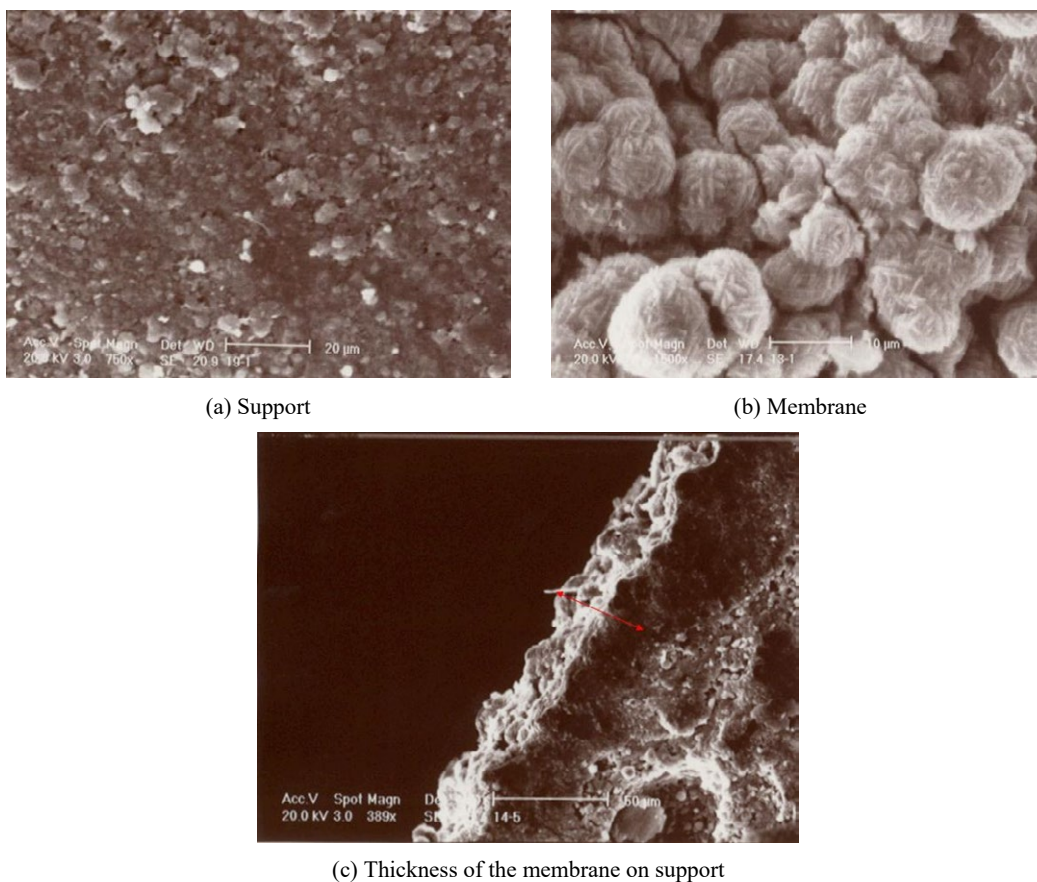(c) Thickness of the membrane on support

Fig. 6: SEM micrograph of the (a) Support, (b) Membrane and (c) Thickness of the membrane on support

Table 3: Cross flow results by zeolite membrane

Run	Concentration of Ethanol in feed (wt %)	P (bar)	Q (l/min)	T (°C)	Flux (kg/m².h)
1	80	1	0.5	20	1.1680
2	80	1	1.5	20	1.5196
3	80	1	3	20	1.905
4	80	1	0.5	20	1.1680
5	80	2	0.5	20	1.520
6	80	3	0.5	20	1.905
7	80	1	0.5	20	1.1680
8	80	1	0.5	40	2.415
9	80	1	0.5	60	2.994

J. Water Environ. Nanotechnol., 3(2): 173-190 Spring 2018

183

COMSOL Multiphysics software version 5.2. FEM was applied by this software for numerical solution of the conservation equations. As observed, a concentration boundary layer is formed on the membrane-feed interface in feed compartment (Fig. 7(b)). At z=0, the water concentration is maximum (10 wt. %). As the feed solution flows in the feed compartment, water moves towards the membrane surface due to the concentration and pressure differences (driving forces). Water concentration on the membrane surface is less than its value at the feed inlet (where water concentration is equal to its initial value, $C_{0,w}$). In fact, the water concentration on the membrane surface was calculated from the membrane selectivity (Eq. 12) and its value in the membrane side. Since water concentration in the membrane is always less than its value in the feed, the water concentration on the membrane-feed boundary ($r=R_2$) is always less than its value in the feed bulk.

Water transfer mechanism through the membrane was described only by diffusion. Since at the membrane-permeate interface the vacuum condition was imposed, the water concentration on this boundary was assumed to be zero (Fig. 7 (a)). Water distribution is highest on the membrane-feed interface, because it is calculated from its value in the feed section, which is always highest (Eq. 18).

Fig. 8 represents the effect of various membrane lengths on the water concentration versus r-coordinate at constant temperature, flow rate and pressure of 60°C, 3 l/min and 1 bar, respectively. Water concentration increases along r direction, as expected. The concentration gradient in feed compartment (Fig. 8 (b)) is great at regions near the membrane-feed interface ($r=R_2$) due to the mass transfer towards the membrane at this region (greater driving force). Concentration reaches a constant value ($C_{0,w}$) at radii more than 7 mm. At regions near the feed entrance (z<L/10) total concentration is higher. This is because that this region is near the feed flow inlet with highest concentration value ($C_{0,w}$). Water distribution within the membrane (Fig. 8 (a)) is linear. Its concentration is zero on the membrane-permeate boundary because of the dry membrane applied on this boundary. In fact the water is vaporized on this region and its concentration reaches zero. Water concentration is highest on feed-membrane interface, as mentioned above.

Fig. 9 demonstrates the concentration profile along z coordinate at constant flow rate (3 l/min) and
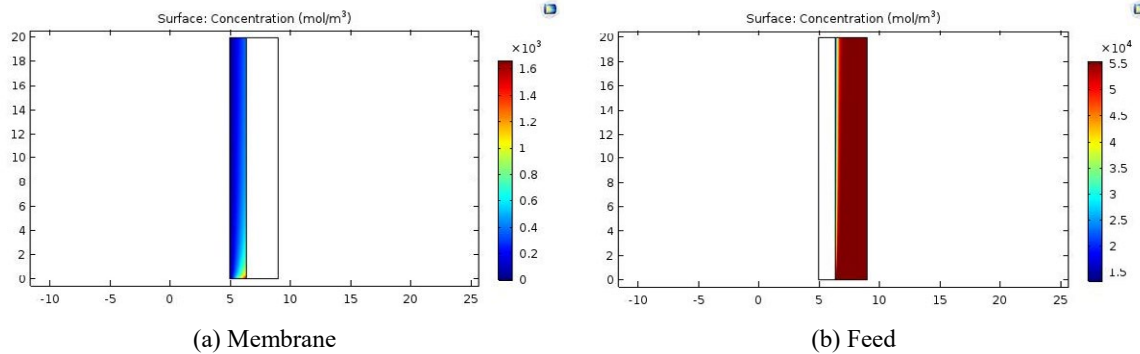

(a) Membrane
(b) Feed

Fig. 7: Concentration distribution of water at 60 °C temperature and 3 l/min feed flow rate (1 bar); (a) Membrane section and (b) Feed section
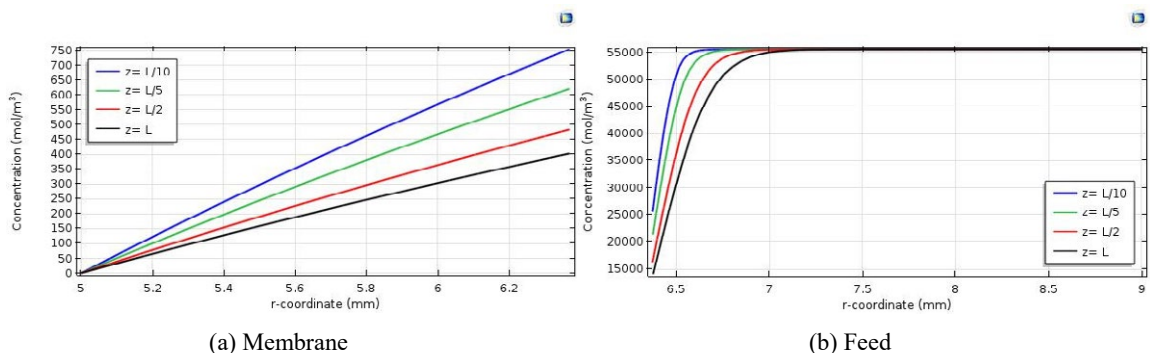

(a) Membrane
(b) Feed

Fig. 8: Water concentration profile vs. r-coordinate at different membrane lengths (60 °C temperature, 1 bar pressure and 3 l/min feed flow rate)

184

J. Water Environ. Nanotechnol., 3(2): 173-190 Spring 2018

different radii. Results indicate that the variation of water concentration along the z coordinate is considerable and that cannot be neglected compared to its variation along r coordinate. The figure also illustrates that the concentration value is greater at membrane module entrance which is due to the greater water concentrations at feed inlet. By moving away from the membrane-feed interface within feed section (Fig. 9(b)), the concentration increases. This behavior can be attributed to less water transfer towards the membrane at regions far from membrane-feed boundary which results in much higher concentration values. Similarly, water distribution within the membrane (Fig. 9(a)) is higher at areas near the feed-membrane interface (R>6 mm).

Figs. 10 and 11 show the effect of various feed flow rates on water concentration distribution within the feed section and the membrane section. As can be seen, water concentration increases with growing feed flow rate. This behavior can be attributed to the fact that higher velocities (or flow
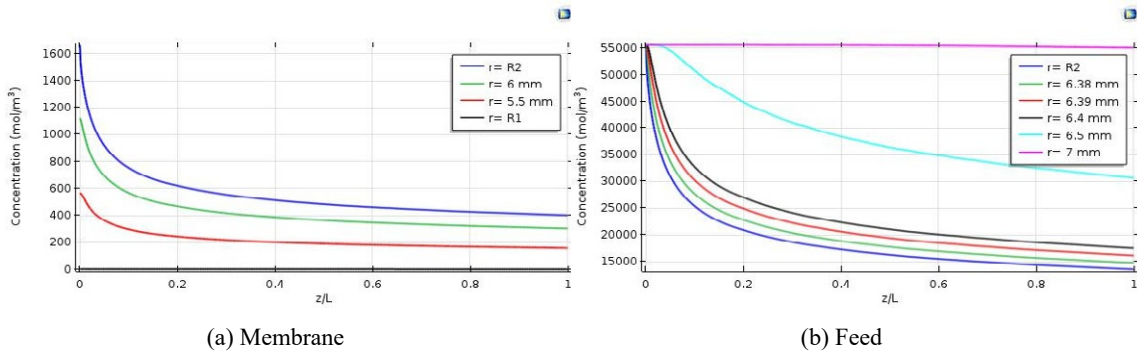

| (a) Membrane | (b) Feed |

Fig. 9: Water concentration distribution vs. dimensionless length at different radii (60 °C temperature, 1 bar pressure and 3 l/min feed flow rate); (a) Membrane section and (b) Feed section
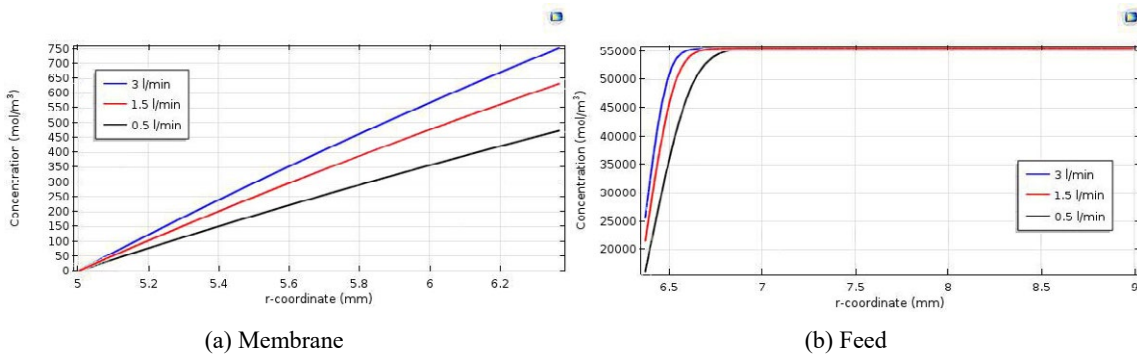

| (a) Membrane | (b) Feed |

Fig. 10: Water concentration profile vs. r-coordinate at different feed flow rates (60 °C temperature and 1 bar pressure); (a) Membrane section and (b) Feed section
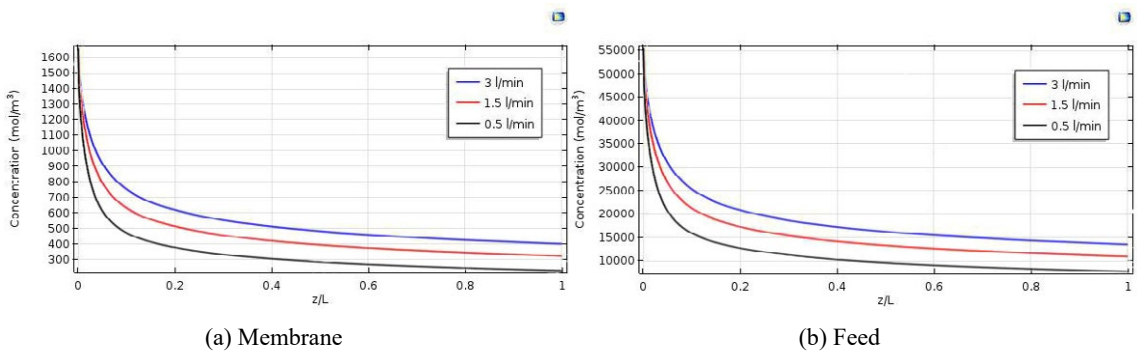

| (a) Membrane | (b) Feed |

Fig. 11: Water concentration profile vs. membrane dimensionless length at different feed flow rates (60 °C temperature and 1 bar pressure); (a) Membrane section and (b) Feed section

rates) would decrease the contact time of the feed flow with membrane and consequently less water has enough time to pass through the membrane. Therefore, much higher concentrations will be obtained at feed compartment and at larger feed flow rates. Similarly, concentration profile grows in membrane segment (Eq. (18)). Hence, it can be concluded that the effective flow rate is 3 l/min, which is in harmony with the experimental results (Table 3).

Fig. 12 and 13 show the effect of temperature on water concentration at different module dimensions. Since the results for concentration distribution vs. r-coordinate at feed segment were almost the same at different temperatures with negligible difference, it is not plotted in Fig. 12. Figures indicate that the temperature has positive effect on concentration profile. In fact, higher temperatures lead to reduced viscosity and density. This decrease in dynamic viscosity and density will result in the smoothness of the feed flow and consequently will lead to an increase in the velocity

magnitude. Greater velocities will lead to higher concentrations, as mentioned in the previous paragraph. Therefore, optimum temperature is 60°C in PV of Ethanol/water mixture, which is exactly the same as what had been reported in the experiments (Table 3).

Velocity distribution

Fig. 14 shows the velocity field in the feed phase of the PV membrane system. The velocity distribution was obtained using numerical solution of momentum balance. This was done by adding a "laminar flow" physic to the whole model in COMSOL. As can be seen from the figure, the velocity profile is fully developed after a short distance. Velocity is zero on the membrane-feed interface and the outer radius of feed section (due to no slip condition) and is highest on the half of the feed section boundary (symmetry condition).

Fig. 15 shows the effect of various membrane lengths on the velocity profile vs. radius in the feed section. As can be seen, the velocity profile is
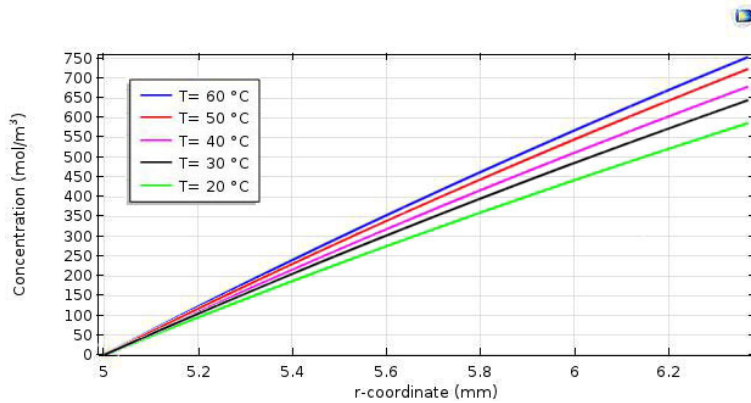

Fig. 12: Water concentration profile within the membrane vs. r-coordinate at different temperatures (3 l/min feed flow rate and 1 bar pressure)

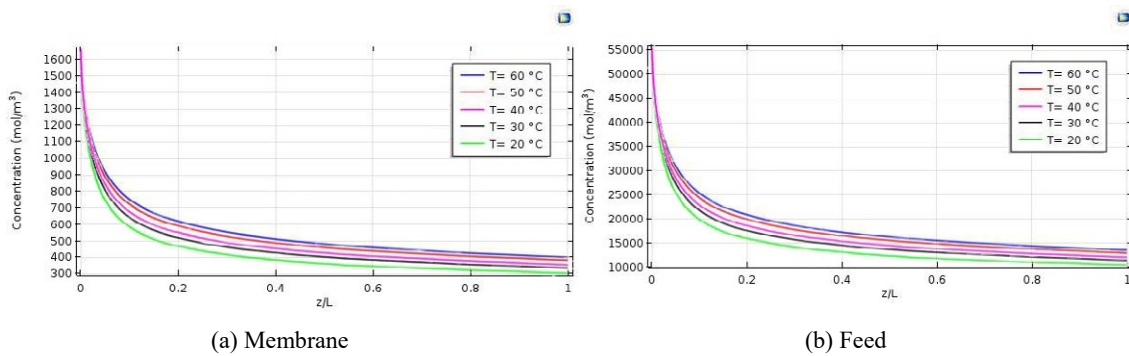| (a) Membrane | (b) Feed |

Fig. 13: Water concentration profile vs. membrane dimensionless length at different temperatures (3 l/min feed flow rate and 1 bar pressure); (a) Membrane section and (b) Feed section
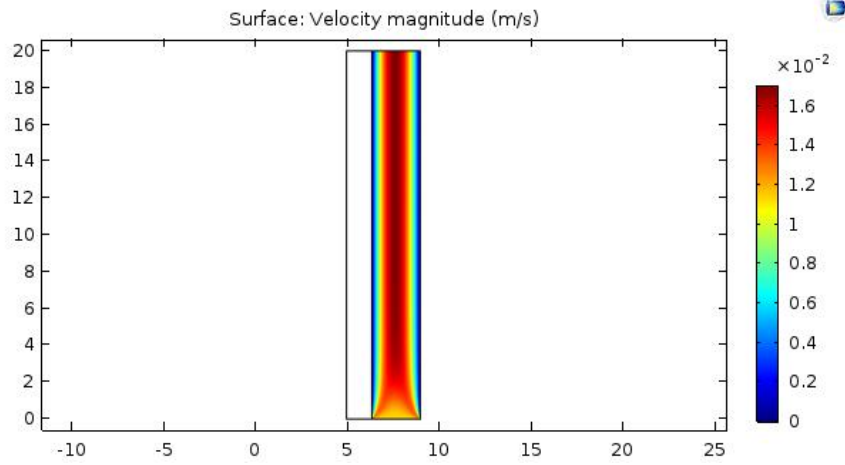
Fig. 14: Velocity profile (60 °C temperature, 3 l/min feed flow rate and 1 bar pressure)
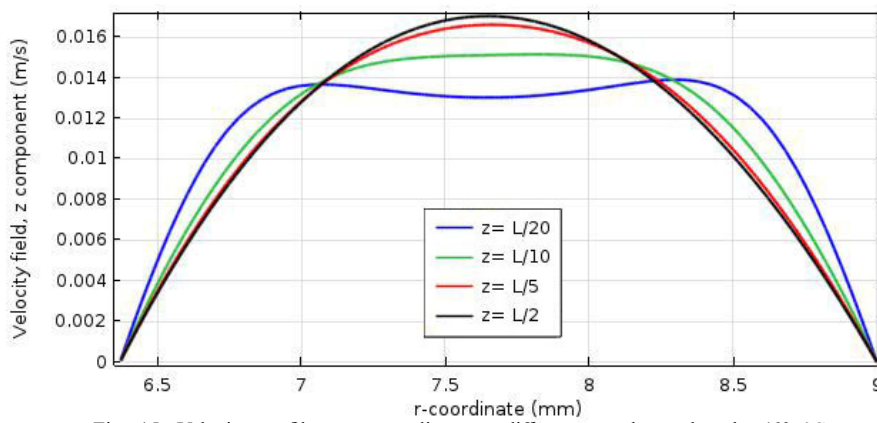

Fig. 15: Velocity profile vs. r-coordinate at different membrane lengths (60 °C temperature, 3 l/min feed flow rate and 1 bar pressure)
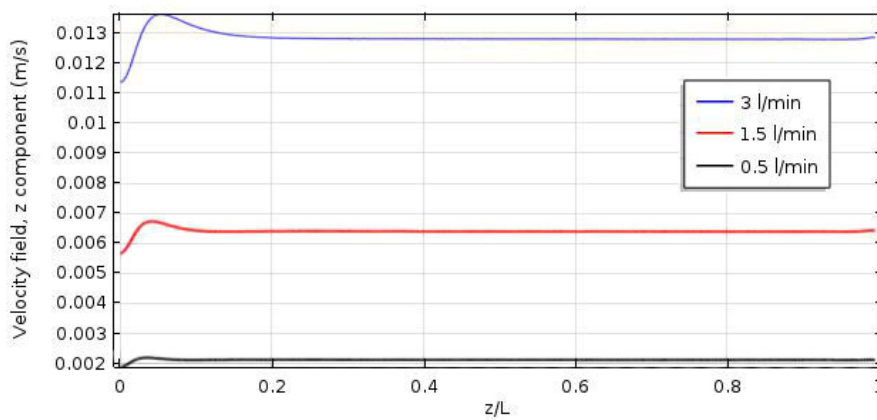

Fig. 16: Velocity profile vs. dimensionless membrane length at different feed flow rates (60 °C temperature and 1 bar pressure)

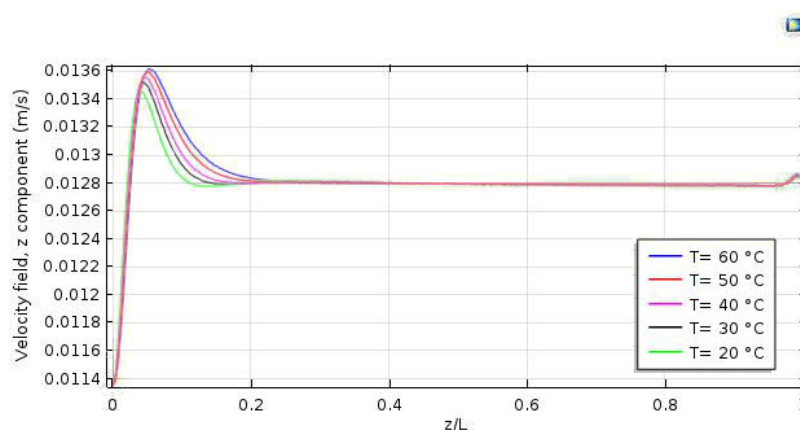*J. Water Environ. Nanotechnol., 3(2): 173-190 Spring 2018*

187

Fig. 17: Velocity profile vs. dimensionless membrane length at different temperatures (3 l/min feed flow rate and 1 bar pressure)

parabolic and becomes fully developed after a short distance (lengths approximately more than L/5). As observed, entrance effects are considered in this simulation, which is one of the advantages of FEM simulation.

Fig. 16 represents the effect of varying feed flow rates on the velocity distribution vs. dimensionless length. Velocity profile is almost parabolic and reaches its maximum value at the regions close to the feed entrance. Maximum velocity magnitude increases with increasing feed flow rate, as expected.

Fig. 17 represents velocity distribution vs. dimensionless length at various temperatures. Maximum velocity magnitude increases slightly with increasing temperature. In fact, an increase in temperature leads to smaller values of density and viscosity of the Ethanol/water solution. As mentioned earlier, reduction of these values leads to a decrease in resistance to flow, so the velocity increases.

CONCLUSION

Nano HS zeolite membranes were synthesized at different gel compositions, times and temperatures. The best range of operating condition (time and temperature) for hydrothermal synthesis of nano-pore HS zeolite membrane were 12-24 h and 70-130°C, respectively. These membranes showed very good membrane performance for separation of Ethanol /water mixtures. It is expected that PV using these membranes can be highly effective for industry, provided that they can be produced cheap at a large scale. Nano HS zeolite membrane was firstly used for dehydration of aqueous Ethanol mixtures. Separation factors as high as 10000 were

obtained at 90 wt.% Ethanol concentration. Effect of operating condition on pervaporation performance showed that increasing pressure, feed rate and temperature increases the flux linearly. Performance of PV system was finally modeled using COMSOL Multiphysics software version 5.2. Modeling was done by solving mass and momentum equations numerically by Finite Element Method (FEM). Effect of varying temperatures, feed flow rates and dimensions on the membrane applicability was investigated. Good modeling results indicated that FEM is a powerful method for modeling membrane separation systems. The optimum temperature and flow rate were also found to be 60°C and 3 l/min, respectively.

CONFLICT OF INTEREST

The authors declare that there are no conflicts of interest regarding the publication of this manuscript.

NOMENCLATURE

$C_{0,w}$	initial water concentration (mol/m³)
C_w	water concentration (mol/m³)
C_{w-f}	water concentration in feed phase (mol/m³)
C_{w-m}	water concentration in membrane phase (mol/m³)
D_w	water diffusion coefficient in feed section (m²/s)
D_m	water diffusion coefficient in membrane (m²/s)
F	feed section

F_b	body force (N)
L	membrane length (mm)
M	membrane section
n	partition coefficient
P	pressure (Pa)
P_{atm}	atmospheric pressure (Pa)
r	radial coordinate
R_1	permeate-membrane radius (mm)
R_2	membrane-feed radius (mm)
R_3	outer radius of the feed section (mm)
R	reaction term (mol/m³.s)
S	selectivity
t	separation time (s)
U	velocity vector (m/s)
u	z-component velocity (m/s)
$x_{Ethanol}$	Ethanol wt.% in feed
x_{water}	water wt.% in feed
$y_{Ethanol}$	Ethanol wt.% in permeate
y_{water}	water wt.% in permeate
z	axial coordinate
ρ	density (kg/m³)
μ	viscosity (Pa.s)

REFERENCES

1. Nour M, Kosaka H, Bady M, Sato S, Abdel-Rahman AK. Combustion and emission characteristics of DI diesel engine fuelled by ethanol injected into the exhaust manifold. Fuel Processing Technology. 2017;164:33-50.

2. Klinov AV, Akberov RR, Fazlyev AR, Farakhov MI. Experimental investigation and modeling through using the solution-diffusion concept of pervaporation dehydration of ethanol and isopropanol by ceramic membranes HybSi. Journal of Membrane Science. 2017;524:321-33.

3. Díaz VHG, Tost GO. Butanol production from lignocellulose by simultaneous fermentation, saccharification, and pervaporation or vacuum evaporation. Bioresource Technology. 2016;218:174-82.

4. Van Hoof V, Dotremont C, Buekenhoudt A. Performance of Mitsui NaA type zeolite membranes for the dehydration of organic solvents in comparison with commercial polymeric pervaporation membranes. Separation and Purification Technology. 2006;48(3):304-9.

5. Amnuaypanich S, Patthana J, Phinyocheep P. Mixed matrix membranes prepared from natural rubber/poly(vinyl alcohol) semi-interpenetrating polymer network (NR/PVA semi-IPN) incorporating with zeolite 4A for the pervaporation dehydration of water–ethanol mixtures. Chemical Engineering Science. 2009;64(23):4908-18.

6. Sato K, Sugimoto K, Nakane T. Preparation of higher flux NaA zeolite membrane on asymmetric porous support and permeation behavior at higher temperatures up to 145°C in vapor permeation. Journal of Membrane Science. 2008;307(2):181-95.

7. Li Y, Chen H, Liu J, Li H, Yang W. Pervaporation and vapor permeation dehydration of Fischer–Tropsch mixed-alcohols by LTA zeolite membranes. Separation and Purification Technology. 2007;57(1):140-6.

8. Xia LL, Li CL, Wang Y. In-situ crosslinked PVA/organosilica hybrid membranes for pervaporation separations. Journal of Membrane Science. 2016;498:263-75.

9. Li Q, Cheng L, Shen J, Shi J, Chen G, Zhao J, et al. Improved ethanol recovery through mixed-matrix membrane with hydrophobic MAF-6 as filler. Separation and Purification Technology. 2017;178:105-12.

10. N. N. Li, J. M. Calo, Separation and Purification Technology, Marcel Dekker, New York, 2nd edition, (1980).

11. Yin H, Lau CY, Rozowski M, Howard C, Xu Y, Lai T, et al. Free-standing ZIF-71/PDMS nanocomposite membranes for the recovery of ethanol and 1-butanol from water through pervaporation. Journal of Membrane Science. 2017;529:286-92.

12. Narkkun T, Jenwiriyakul W, Amnuaypanich S. Corrigendum to "Dehydration performance of double-network poly(vinyl alcohol) nanocomposite membranes (PVAs-DN)" [J. Membr. Sci. 528 (2017) 284–295]. Journal of Membrane Science. 2017;530:146.

13. Jiang J, Wang L, Peng L, Cai C, Zhang C, Wang X, et al. Preparation and characterization of high performance CHA zeolite membranes from clear solution. Journal of Membrane Science. 2017;527:51-9.

14. Santoro S, Galiano F, Jansen JC, Figoli A. Strategy for scale-up of SBS pervaporation membranes for ethanol recovery from diluted aqueous solutions. Separation and Purification Technology. 2017;176:252-61.

15. Pera-Titus M, Llorens J, Tejero J, Cunill F. Description of the pervaporation dehydration performance of A-type zeolite membranes: A modeling approach based on the Maxwell–Stefan theory. Catalysis Today. 2006;118(1-2):73-84.

16. Yu L, Zeng C, Wang C, Zhang L. In situ impregnation–gelation–hydrothermal crystallization synthesis of hollow fiber zeolite NaA membrane. Microporous and Mesoporous Materials. 2017;244:278-83.

17. Kondo M, Kita H. Permeation mechanism through zeolite NaA and T-type membranes for practical dehydration of organic solvents. Journal of Membrane Science. 2010;361(1-2):223-31.

18. Sorenson SG, Payzant EA, Gibbons WT, Soydas B, Kita H, Noble RD, et al. Influence of zeolite crystal expansion/contraction on NaA zeolite membrane separations. Journal of Membrane Science. 2011;366(1-2):413-20.

19. Liu G, Jiang Z, Cao K, Nair S, Cheng X, Zhao J, et al. Pervaporation performance comparison of hybrid membranes filled with two-dimensional ZIF-L nanosheets and zero-dimensional ZIF-8 nanoparticles. Journal of Membrane Science. 2017;523:185-96.

J. Water Environ. Nanotechnol., 3(2): 173-190 Spring 2018

189

20. Qu H, Kong Y, Lv H, Zhang Y, Yang J, Shi D. Effect of crosslinking on sorption, diffusion and pervaporation of gasoline components in hydroxyethyl cellulose membranes. Chemical Engineering Journal. 2010;157(1):60-6.

21. Lin L, Zhang Y, Kong Y. Pervaporation separation of n-heptane/thiophene mixtures by polyethylene glycol membranes: Modeling and experimental. Journal of Colloid and Interface Science. 2009;339(1):152-9.

22. Das P, Ray SK. Analysis of sorption and permeation of acetic acid–water mixtures through unfilled and filled blend membranes. Separation and Purification Technology. 2013;116:433-47.

23. Das P, Ray SK. Pervaporative recovery of tetrahydrofuran from water with plasticized and filled polyvinylchloride membranes. Journal of Industrial and Engineering Chemistry. 2016;34:321-36.

24. Moulik S, Kumar KP, Bohra S, Sridhar S. Pervaporation performance of PPO membranes in dehydration of highly hazardous mmh and udmh liquid propellants. Journal of Hazardous Materials. 2015;288:69-79.

25. Samei M, Iravaninia M, Mohammadi T, Asadi AA. Solution diffusion modeling of a composite PVA/fumed silica ceramic supported membrane. Chemical Engineering and Processing: Process Intensification. 2016;109:11-9.

26. Rezakazemi M, Shahverdi M, Shirazian S, Mohammadi T, Pak A. CFD simulation of water removal from water/ethylene glycol mixtures by pervaporation. Chemical Engineering Journal. 2011;168(1):60-7.

27. Rom A, Miltner A, Wukovits W, Friedl A. Energy saving potential of hybrid membrane and distillation process in butanol purification: Experiments, modelling and simulation. Chemical Engineering and Processing: Process Intensification. 2016;104:201-11.

28. Liu D, Liu G, Meng L, Dong Z, Huang K, Jin W. Hollow fiber modules with ceramic-supported PDMS composite membranes for pervaporation recovery of bio-butanol. Separation and Purification Technology. 2015;146:24-32.

29. Jain M, Attarde D, Gupta SK. Removal of thiophenes from FCC gasoline by using a hollow fiber pervaporation module: Modeling, validation, and influence of module dimensions and flow directions. Chemical Engineering Journal. 2017;308:632-48.

30. Moulik S, Nazia S, Vani B, Sridhar S. Pervaporation separation of acetic acid/water mixtures through sodium alginate/polyaniline polyion complex membrane. Separation

31. Qiao Z, Wu Y, Li X, Zhou J. Molecular simulation on the separation of water/ethanol azeotropic mixture by poly(vinyl alcohol) membrane. Fluid Phase Equilibria. 2011;302(1-2):14-20.

32. Mafi A, Raisi A, Hatam M, Aroujalian A. A mathematical model for mass transfer in hydrophobic pervaporation for organic compounds separation from aqueous solutions. Journal of Membrane Science. 2012;423-424:175-88.

33. Villaluenga J, Cohen Y. Numerical model of non-isothermal pervaporation in a rectangular channel. Journal of Membrane Science. 2005;260(1-2):119-30.

34. Kazemimoghadam M, Pak A, Mohammadi T. Dehydration of water/1-1-dimethylhydrazine mixtures by zeolite membranes. Microporous and Mesoporous Materials. 2004;70(1-3):127-34.

35. K. Speronello., 1986- Porous mullite, U.S. Patent NO 4628042.

36. K. Speronello., 1986- Porous mullite, U.S. Patent No. 4601997.37. Coronas J. Present and future synthesis challenges for zeolites. Chemical Engineering Journal. 2010;156(2):236-42.

38. Cho CH, Oh KY, Kim SK, Yeo JG, Lee YM. Improvement in thermal stability of NaA zeolite composite membrane by control of intermediate layer structure. Journal of Membrane Science. 2011;366(1-2):229-36.

39. Cho CH, Oh KY, Yeo JG, Kim SK, Lee YM. Synthesis, ethanol dehydration and thermal stability of NaA zeolite/alumina composite membranes with narrow non-zeolitic pores and thin intermediate layer. Journal of Membrane Science. 2010;364(1-2):138-48.

40. Aguado S, Gascón J, Jansen JC, Kapteijn F. Continuous synthesis of NaA zeolite membranes. Microporous and Mesoporous Materials. 2009;120(1-2):170-6.

41. Kazemimoghadam M, Mohammadi T. Preparation of nano pore hydroxysodalite zeolite membranes using of kaolin clay and chemical sources. Desalination. 2011;278(1-3):438-42.

42. Kazemimoghadam M, Mohammadi T. Preparation of mordenite membranes for dehydration of water–UDMH. Desalination. 2010;260(1-3):276-9.

43. Transport phenomena, R. B. Bird, W. E. Stewart, and E. N. Lightfoot, John Wiley and Sons, Inc., New York(1960). 780 pages.$11.50. AIChE Journal. 1961;7(2):5J-6J.

44. Kazemimoghadam M. Preparation of nanopore HS zeolite membranes for reverse osmosis processes. Desalination and Water Treatment. 2011;30(1-3):51-7.

190

J. Water Environ. Nanotechnol., 3(2): 173-190 Spring 2018